Lineshape Fitting of Deuterium Magic Angle Spinning Spectra of Paramagnetic Compounds in Slow and Fast Limit Motion Regimes

Hyerim Lee,[§] Tatyana Polenova,[§] Robert H. Beer,[†] and Ann E. McDermott*,[§]

Contribution from the Chemistry Department, Columbia University, New York, New York 10027, and Department of Chemistry, Fordham University, Bronx, New York 10458

Received March 1, 1999. Revised Manuscript Received May 18, 1999

Abstract: Deuterium solid-state NMR spectra of paramagnetic compounds can be used to study metal−ligand geometry, spin couplings, and conformational dynamics. We report spinning sideband intensity simulations of temperature-dependent deuterium magic angle spinning spectra of paramagnetic complexes based upon straightforward application of the Herzfeld−Berger type routines. We adopt a point dipole description of the anisotropic hyperfine interaction and utilize an isotropic $\tilde{\mathbf{g}}$ tensor. Despite these simplifications, we demonstrate that fine structure constants, including electron−nuclear dipolar coupling and mutual orientation of the dipolar and quadrupolar tensors, can be determined on the basis of the simulations within 0.5 Å and 20°, respectively. These simulations have sufficient sensitivity to detect the electron−nuclear dipolar couplings as weak as 5 kHz, which corresponds to the distance between the metal and the deuteron(s) of 3 Å for $S = {}^1/_2$ or 6.5 Å for $S = {}^5/_2$.

Introduction

Many recent studies demonstrate the promise of deuterium NMR spectroscopy of paramagnetic systems for addressing local molecular geometry and conformational dynamics. Deuterium NMR of solids, either diamagnetic or paramagnetic, is one of the most informative techniques for probing dynamics on a variety of time scales;[1] it has been successfully applied in many systems, from small inorganic substances to biological macromolecules including both static and magic angle spinning (MAS) measurements.[2] Solid-state (SS) deuterium MAS NMR spectra exhibit both the sensitivity and the resolution to be useful for probing biological paramagnetic systems.[1−3] Deuterium lineshape simulations in paramagnetic static samples have been reported,[1,4] and estimated dipolar hyperfine couplings from solid-state NMR MAS data have been used previously for chemical analysis.[5] A pulse sequence involving MAS has been developed that allows separation of local interactions and independently assesses the quadrupole and the paramagnetic shift tensors.[6] This report concerns details of the interpretation of the lineshapes of deuterium spectra in paramagnetic compounds during the MAS experiments, and determination of the metal-nuclear geometry and conformational dynamics, based on the Herzfeld−Berger type expressions,[7] as had been done for ^{2}H MAS of diamagnetic substances already.[8]

Typically, the spectral lineshape for a deuteron in a randomly oriented diamagnetic solid is a Pake pattern.[9] Due to the fact that deuterons are an $I = 1$ system, this spectrum reflects two transitions. Their quadrupolar lineshapes are mirror images of one another, and the net spectrum is symmetric about the center frequency. However, in the presence of paramagnetic centers, the deuterium lineshape is no longer symmetric due to the anisotropic dipolar interaction between a deuteron and the thermally averaged magnetic moments of the unpaired electrons (Figure 1), which affects both transitions in a similar way. The net frequency depends on the sum of the dipolar and quadrupolar interactions, and thus the lineshape depends on the relative orientation of their two tensor axes.[10] As a consequence, the lineshape can provide information about electron−nuclear couplings. As elaborated in this paper, molecular motion has the tendency to "foreshorten" the quadrupolar tensor but not the dipolar tensor; thus, for systems in fast conformational exchange, severely distorted lineshapes are expected and were observed.

We conducted simulations of the spinning sideband intensities in ^{2}H MAS spectra for ligand-deuterated, crystallographically characterized paramagnetic compounds to demonstrate the agreement between the calculated and the experimental spectra of model compounds. The simulations were carried out on the basis of several assumptions, which simplify the tensor manipulations:

(1) The anisotropic part of the electron−deuteron coupling is a purely through-space, direct dipolar interaction. The contact term in the electron−nuclear coupling is also strong but will affect only the isotropic component of the frequency, which can be treated separately and is not a subject of this study.

* To whom correspondence should be addressed.
§ Columbia University.
† Fordham University.

(1) Lin, T.-H.; DiNatale, J. A.; Vold, R. R. *J. Am. Chem. Soc.* **1994**, *116*, 2133−2134.
(2) Liu, K.; Williams, J.; Lee, H.; Fitzgerald, M. M.; Jensen, G. M.; Goodin, D. B.; McDermott, A. E. *J. Am. Chem. Soc.* **1998**, *120*, 10199−10202.
(3) Lee, H.; Ortiz de Montellano, P. R.; McDermott, A. E. *Biochemistry*, in press.
(4) Siminovitch, D. J.; Rance, M.; Jeffrey, K. R.; Brown, M. F. *J. Magn. Reson.* **1984**, *58*, 62−75.
(5) Brough, A. R.; Grey, C. P.; Dobson, C. M. *J. Am. Chem. Soc.* **1993**, *115*, 7318−7327.
(6) Spaniol, T. P.; Kubo, A.; Terao, T. *J. Chem. Phys.* **1997**, *106*, 5393−5405.
(7) Herzfeld, J.; Berger, A. E. *J. Chem. Phys.* **1980**, *73*, 6021−6030.
(8) Kristensen, J. H.; Bildsøe, H.; Jakobsen, H. J.; Nielsen, N. C. *J. Magn. Reson.* **1991**, *92*, 443−453.
(9) Pake, G. E. *J. Chem. Phys.* **1948**, *16*, 327−336.
(10) Nayeem, A.; Yesinowski, J. P. *J. Chem. Phys.* **1988**, *89*, 4600−4608.

10.1021/ja990636u CCC: $18.00
Published on Web 07/14/1999

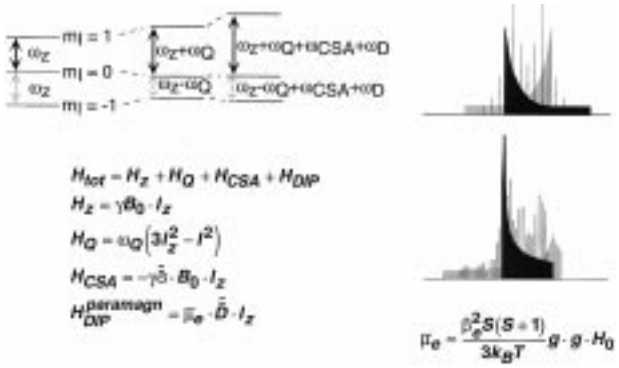

Figure 1. Interaction Hamiltonian and energy level diagram for an $I = 1$ deuterium in the presence of a local unpaired electron. $\bar{\mu}_e = [\beta^2 S(S + 1)/3k_BT]g^2 \cdot H_0$ is a description for the thermally averaged mean magnetic moment of two electron states. On the right, a static lineshape for deuterons in diamagnetic (top) and paramagnetic (bottom) compounds are indicated overlaid with MAS stick spectra.

(2) The electronic magnetic moment is localized at the metal, and a point dipole approximation can be used to describe the dipolar interaction.

(3) The electron−nuclear interaction was described with a second rank tensor, i.e., the *g* anisotropy was omitted.

(4) Only one nearby metal−metal cluster was taken into consideration (neighboring sites in lattice and neighboring molecules were ignored).

Two types of deuterons were studied: the $-CD_3$ group in the fast motion limit of the three-site hop and the −CD or ND group in the static limit. Euler angles relating the dipolar hyperfine and electric quadrupolar interactions were obtained from the respective crystal structures. In this report, we compare simulated and experimental spectra and demonstrate that good agreement can be achieved despite the use of these simplifying assumptions.

Experimental Section

Simulations were performed using Mathematica 3.0 (Wolfram, Inc.). Lineshape fitting was performed for five different paramagnetic compounds: V^{III}(acac-3-*d*)$_3$, Cu^{II}(DL-alanine -*Nd*$_2$)$_2$·D_2O, Mn^{III}(acac-3-*d*)$_3$, Fe^{III}(salen)(OAc-d_3), and Fe^{III}(salNiPr-*d*)Cl_3. These compounds have been characterized by X-ray crystallography; therefore, the distance from metal center to deuterium and the relative orientations of the deuterium bond and the metal−deuterium vector are known. The mutual orientations of the dipolar and quadrupolar tensors (assuming that both tensors are axially symmetric) can be described using a polar angle θ as shown below:

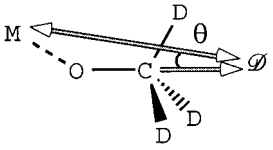

where M is the metal, *D* is the motionally averaged deuterium, and θ is the angle between the *z*-components of the dipolar and quadrupolar tensors.

Information about the local geometry and mutual tensor orientation for the compounds under study is summarized in Table 1. The quadrupolar tensors for the rigid C−D and the fast limit CD_3 groups are uniaxial to a very good approximation: only a single polar angle (and a center-to-center distance) was used to describe their mutual orientations for most cases.

Calculations of ^2H Solid-State Magic Angle Spinning NMR Spectra of Paramagnetic Solids. Deuterium MAS NMR spectra of paramagnetic solids are influenced by the nuclear quadrupolar interaction and the electron−nuclear dipolar interaction. The total interaction Hamiltonian of a spin $I = 1$ in paramagnetic systems can be expressed as follows:

$$H_{TOT} = H_Z + H_{CSA} + H_Q + H_{DIP} \quad (1)$$

where

$$H_Z = g\cdot\mathbf{B}_0\cdot I_z \quad (2)$$

$$H_Q = \omega_Q(3I_z^2 - I^2) \quad (3)$$

$$H_{CSA} = \gamma\tilde{\sigma}\cdot\mathbf{B}_0\cdot I_z \quad (4)$$

$$H_{DIP}^{paramagn} = \bar{\mu}_e\cdot\tilde{D}\cdot I_z = \omega_D\cdot I_z \quad (5)$$

where $\omega_Q/2\pi = e^2qQ/\hbar$, and $\omega_D/2\pi = (\mu_0/4\pi)\cdot\mu_{eff}\cdot\gamma_D\cdot r^{-3}$. In the expression for $\omega_D/2\pi$, μ_{eff} is the effective magnetic moment of the electron, $\mu_{eff} = \beta_e^2\cdot s(s+1)\cdot g^2\cdot H/(3k_BT)$, where $g = 2$; *r* is the distance between the metal and the deuteron (10^{-10} m); *s* is the electron spin state; *H* is the magnetic field strength, $H = 9.35$ T; β_e is the Bohr magneton, $\beta_e = 9.27 \times 10^{-24}$ J·T^{-1}; k_B is the Boltzmann constant, $k_B = 1.38 \times 10^{-23}$ J·K^{-1}; μ_0 is the permeability of vacuum, $\mu_0 = 4\pi \times 10^{-7}$ kg·m·s^{-2}·A^{-2}; γ_D is the gyromagnetic ratio of a deuteron, $\gamma_D = 2.675 \times 10^8$ (60/400) rad^{-1}·T^{-1}; $\hbar$ is the Planck constant, $\hbar = 6.626 \times 10^{-34}$ J·s; and *T* is the temperature, $T = 300$ K (23 °C) or 233 K (−40 °C). This Hamiltonian is truncated, and additional approximations are made so that only the terms involving the parts of the dipolar and the nuclear quadrupolar interactions that commute with the Zeeman interaction are preserved.

The spin Hamiltonian due to the dipolar coupling between a nuclear moment and an electron moment is written as

$$H_{DIP} = \bar{\mu}_e\cdot\tilde{D}\cdot I_z \quad (6)$$

where $\bar{\mu}_e = [\beta^2 S(S + 1)/3k_BT\,]g^2\cdot H_0$ is the thermally averaged mean magnetic moment of the paramagnetic ion, as described by Bloembergen.[11] The thermally averaged form of the electron magnetic dipole moment can be used instead of its operator form due to the electron spin relaxation, which is fast on the NMR time scale. The *g*-anisotropy enters into the expression as a tensorial quantity. However, for the purpose of our simulations, we kept only the isotropic part of the tensor, which is a good approximation for some of the paramagnetic molecules of interest [V^{III}(acac-3-*d*)$_3$, Cu^{II}(DL-alanine-*Nd*$_2$)$_2$·D_2O] but probably not for others [Mn^{III}(acac-3-*d*)$_3$, Fe^{III}(salNiPr-*d*)Cl_3, Fe^{III}(salen)(OAc-d_3)]. The use of isotropic *g* factors was probably the most severe approximation in this work (see Discussion section). We decided to use this representation for the initial stages of this study, since introducing additional free parameters would complicate the data analysis substantially and may not be beneficial for obtaining an initial qualitative picture. Strong electron−electron interactions in the neat crystalline solids lead to exchange-broadened lineshape and effectively make this assumption more valid.

The deuterium MAS spectra in the laboratory frame include two transitions: the $m_I = 0$ to 1 transition, whose fine structure involves the sum $\tilde{\Sigma} = +\tilde{Q} + \tilde{D}$, and the $m_I = -1$ to 0 transition, whose fine

Table 1. Parameters Describing the Molecular Geometry of the Model Compound Used in This Study (Taken from the X-ray Crystal Structures)

compound	metal−deuterium distance (Å)	polar angle θ^a	spin state
V^{III}(acac-3-*d*)$_3$	4.2	0	1
Cu^{II}(DL-alanine-*Nd*$_2$)$_2$·D_2O	2.4	48 or 52	$^1/_2$
Mn^{III}(acac-3-*d*)$_3$	4.3	$<10^b$	2
Fe^{III}(salen)(OAc-d_3)^c	4.7, 3.45, 3.61	8.91, 90.5, 82.5	$^5/_2$
Fe^{III}(salNiPr-*d*)Cl_3	3.4	30	$^5/_2$

[a] Describing the relative orientation of the quadrupolar and the dipolar tensors. [b] Varied among two types of crystal packing existed for Mn^{III}(acac-3-d_3). [c] For each of the deuterons in the methyl group.

(11) Bloembergen, N. *Physica* **1950**, *16*, 95−112.

structure involves the difference $\tilde{\Delta} = -\tilde{Q} + \tilde{D}$ of the quadrupolar ($\tilde{Q}$) and the dipolar ($\tilde{D}$) frequencies (see Figure 1). The two transitions can be treated independently and added to form the final spectrum due to the high-field regime, corresponding to the experimental conditions. The high-field limit results in negligible contributions of the off-diagonal elements of the complete Hamiltonian matrix, thereby allowing for treating the two sub-blocks, containing the two transitions, separately. The spectra were calculated by performing a series of coordinate transformations that bring the quadrupolar and the dipolar tensors first into their common reference frame (crystal fixed frame, CFF, chosen to be the principal axes system of the quadrupolar tensor), where the sum and the difference tensors are computed. Subsequently, the sum and the difference tensors are transformed into their diagonal frames (principal axes system, PAS). This is illustrated below (eqs 7−10):

$$\tilde{\Sigma}^{\mathrm{CFF}} = R^{\mathrm{CFF}}(\alpha',\beta',\gamma')\tilde{D}^{\mathrm{PAS}}(R^{\mathrm{CFF}}(\alpha',\beta',\gamma'))^{-1} + \tilde{\mathrm{Q}}^{\mathrm{PAS}} \quad (7)$$

$$\tilde{\Delta}^{\mathrm{CFF}} = R^{\mathrm{CFF}}(\alpha',\beta',\gamma')\tilde{D}^{\mathrm{PAS}}(R^{\mathrm{CFF}}(\alpha',\beta',\gamma'))^{-1} - \tilde{\mathrm{Q}}^{\mathrm{PAS}} \quad (8)$$

$$\tilde{\Sigma}^{\mathrm{PAS}}(\alpha'',\beta'',\gamma'') = R^{\mathrm{PAS}}(\alpha'',\beta'',\gamma'')\tilde{\Sigma}^{\mathrm{CFF}}(R^{\mathrm{PAS}}(\alpha'',\beta'',\gamma''))^{-1} \quad (9)$$

$$\tilde{\Delta}^{\mathrm{PAS}}(\alpha'',\beta'',\gamma'') = R^{\mathrm{PAS}}(\alpha'',\beta'',\gamma'')\tilde{\Delta}^{\mathrm{CFF}}(R^{\mathrm{PAS}}(\alpha'',\beta'',\gamma''))^{-1} \quad (10)$$

The spinning sideband intensities were computed according to the method of Herzfeld and Berger,[7] separately for each of the two transitions (sum and difference transitions, described above):

$$I_N(\alpha,\beta,\gamma) = f^*(\gamma)\, \mathrm{e}^{i\gamma N} F(\gamma') \quad (11)$$

where $I_N(\alpha,\beta,\gamma)$ is the intensity of the Nth spinning sideband (counting from the centerband, which corresponds to the isotropic part of the combined tensor) for a single molecule, whose orientation is described by the Euler angles α, β, and γ with regard to the rotor frame. The functions F and f are defined as follows:

$$f^*(\gamma) = \mathrm{e}^{(i/\omega_r)(C_1\sin\gamma + (1/2)C_2\sin 2\gamma - S_1\cos\gamma - (1/2)S_2\cos 2\gamma)} \quad (12)$$

$$F(\gamma') = \frac{1}{2\pi}\int_0^{2\pi} \mathrm{e}^{-i\gamma' N} f^*(\gamma')\, \mathrm{d}\gamma' \quad (13)$$

where

$$f^*(\gamma') = \mathrm{e}^{(i/\omega_r)(C_1\sin\gamma + (1/2)C_2\sin 2\gamma - S_1\cos\gamma - (1/2)S_2\cos 2\gamma)} \quad (14)$$

and $\gamma' = \gamma + \omega_r t$,where ω_r is the rotor spinning speed.

The coefficients C_1, C_2, S_1, and S_2 depend on the averaged tensor and the geometry of the molecule in the rotor as described previously:[7]

$$C_1(\alpha,\beta) = -\delta\frac{\sqrt{2}}{2}\sin 2\beta\left(1 + \frac{1}{3}\eta\cos 2\alpha\right) \quad (15)$$

$$C_2(\alpha,\beta) = \delta\left\{\frac{1}{2}\sin^2\beta - \frac{1}{6}\eta(1+\cos^2\beta)\cos 2\alpha\right\} \quad (16)$$

$$S_1(\alpha,\beta) = \delta\eta\frac{\sqrt{2}}{3}\sin\beta\sin 2\alpha \quad (17)$$

$$S_2(\alpha,\beta) = \delta\eta\frac{\sqrt{1}}{3}\cos\beta\sin 2\alpha \quad (18)$$

where δ and η are the anisotropy and the asymmetry parameters of the combined quadrupolar−dipolar tensors (sum $\tilde{\Sigma} = \tilde{Q} + \tilde{D}$ or difference $\tilde{\Delta} = -\tilde{Q} + \tilde{D}$ tensors corresponding to each of the two transitions) in the diagonal representation (PAS) of the combined tensor: $\delta = \Sigma_{zz}$ (or $\delta = \Delta_{zz}$), and $\eta = (\Sigma_{yy} - \Sigma_{xx})/\Sigma_{zz}$ (or $\eta = (\Delta_{yy} - \Delta_{xx})/\Delta_{zz}$).

The powder average of an ensemble of randomly oriented crystallites was calculated by discrete sampling of a random set of orientations (a total of 300 orientations):

$$I_N = \frac{1}{2}\sum_{\alpha,\beta,\gamma}\sin I_N(\alpha,\beta,\gamma)\Delta\beta \quad (19)$$

After powder averaging, the intensities were convolved with a Gaussian lineshape function assuming a width of 50 Hz for each individual spinning sideband (close to the experimental linewidth).

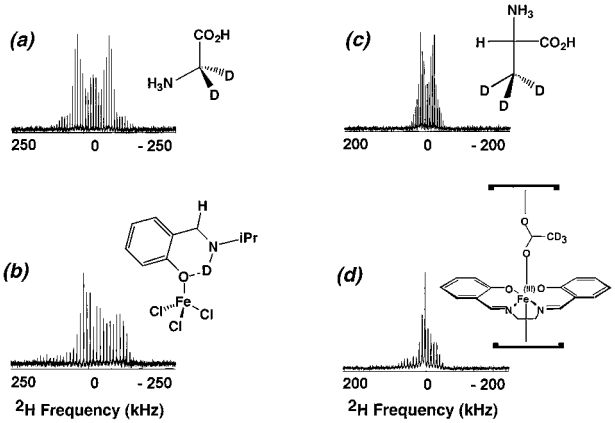

Figure 2. Experimental ^{2}H MAS spectra contrasting the lineshapes for diamagnetic and paramagnetic compounds. The two spectra on the left represent the static limit case for deuterons (no molecular motion, $\omega_Q/2\pi = 167$ kHz), for the following compounds: (a) d_2-glycine (diamagnetic) and (b) *N*-isopropylsalicylaldiminato-*d*-iron trichloride (paramagnetic). The two spectra on the right illustrate the deuterium lineshape in the presence of fast limit, high-symmetry molecular motion, namely methyl groups undergoing a three-site hop ($\omega_Q/2\pi = 56$ kHz) in the following compounds: (c) d_3-alanine (diamagnetic) and (d) *N*,*N*′-ethylenebis(salicylaldiminato))acetato-d_3-iron(III) (paramagnetic). The deuterons in spectra c and d exhibit three-site hops which cause motional averaging of the quadrupolar tensor. The diamagnetic compounds have spectra symmetric about $\omega = 0$, whereas the paramagnetic compounds show asymmetric spectra.

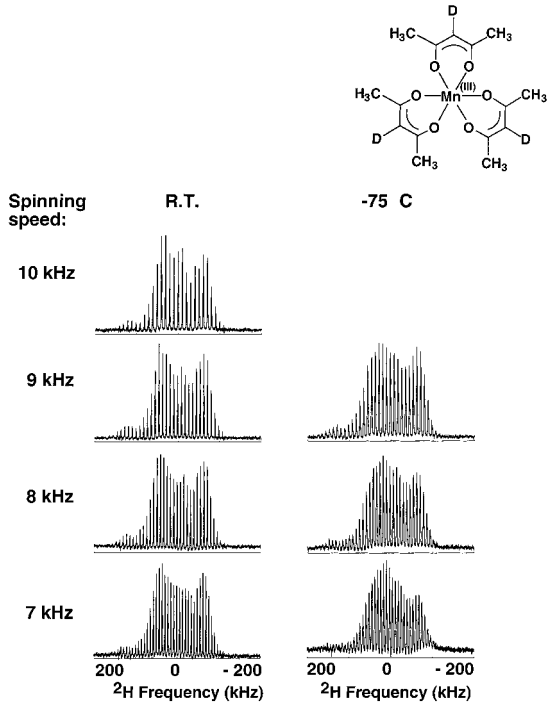

Figure 3. ^{2}H MAS NMR experimental spectra of tris(acetylacetonato-d_3)manganese(III) at 7, 8, 9, and 10 kHz and two temperatures (room temperature and −75 °C). Data were collected using a chemical shift echo pulse sequence, with the 180° pulse synchronized with the first rotor echo. The temperature and spinning speed strongly affect the lineshape of ^{2}H NMR.

If fast-limit high-symmetry motions (i.e., a three-site hop of a CD_3 group) are present in the molecule, the quadrupolar and the electron−nuclear dipolar interactions (and in the general case, other second rank tensorial interactions) for the symmetry-related sites are averaged in a common frame, resulting in an effective interaction tensor that is usually

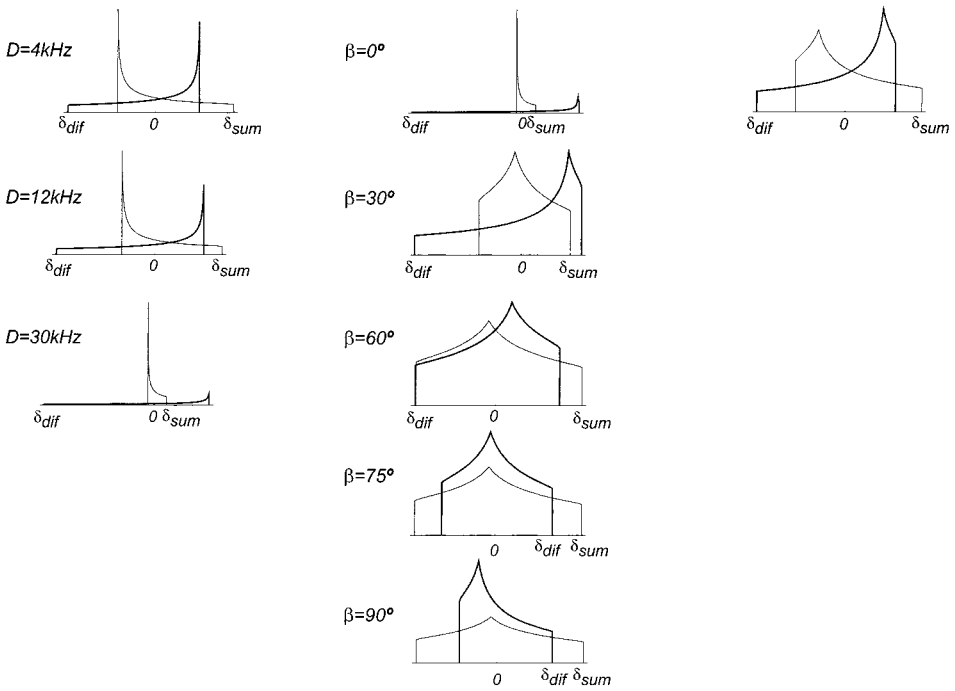

Figure 4. ^2H static lineshape simulated for paramagnetic compounds (1) as a function of a dipolar coupling strength (left column), which ranged from 4 to 30 kHz, using the quadrupolar coupling constant $\omega_Q/2\pi = 167$ kHz and assuming the two tensors to be 0° with respect to each other, (2) as a function of the mutual tensor orientation from 0° to 90° for a given dipolar coupling strength, 50 kHz (middle column), and (3) for a rhombic quadrupolar tensor (right column), a quadrupolar coupling constant $\omega_Q/2\pi = 190$ kHz, asymmetry parameter $\eta = 0.1$, and a dipolar coupling constant of 10 kHz when the two tensors are 35° with respect to each other.

dramatically narrower:[12]

$$\bar{Q} = \frac{1}{N}\sum_{i=1}^{N} R_i^{-1}(\alpha_i,\beta_i,\gamma_i)\cdot\tilde{Q}\cdot R_i(\alpha_i,\beta_i,\gamma_i) \qquad (20)$$

where $\tilde{Q}$ is the quadrupolar tensor in the PAS, and $R_i(\alpha_i,\beta_i,\gamma_i)$ takes each site from the PAS into CFF. In the paramagnetic molecules under study, fast limit motions (i.e., the CD_3 group in Fe^{III}(salen)(OAc-d_3)) will average the quadrupolar tensor as described by eq 20, and a completely analogous expression holds also for the average or effective dipolar tensor, but the motion will have a much weaker effect on the dipolar tensor, due to geometric considerations: the dipolar vectors are related by an acute angle and are nearly collinear as the metal becomes farther away, while the quadrupolar tensors are typically related by high symmetry and by more obtuse subtended angles, as illustrated below:

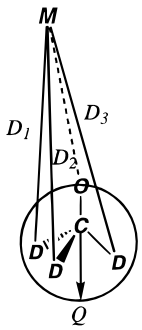

The fast limit spectra were calculated as described above, using the average quadrupolar tensor and an effective dipolar tensor.

Calculations of Static ^2H Lineshapes for Pramagnetic Solids. Static deuterium lineshapes were calculated separately for the two transitions: the $m_I = 0$ to 1 transition, whose fine structure involves the sum $\tilde{\Sigma} = +\tilde{Q} + \tilde{D}$, and the $m_I = -1$ to 0 transition, whose fine structure involves the difference $\tilde{\Delta} = -\tilde{Q} + \tilde{D}$ of the quadrupolar ($\tilde{Q}$) and the dipolar ($\tilde{D}$) frequencies (see Figure 1). The sum and the difference tensors were computed in the common reference frame (CFF) and subsequently diagonalized to obtain the anisotropy and asymmetry parameters. The anisotropic lineshapes were calculated according to Haeberlen.[13] Axially symmetric and rhombic tensors give rise to different expressions for the lineshapes. For an uniaxial tensor, the lineshape is an analytic function of the resonance frequency:

$$I(\omega) = \frac{1}{\sqrt{3}\delta}\frac{1}{[1 + (2\omega/\delta)]^{1/2}} \qquad (21)$$

where $I(\omega)$ is the resonance intensity and δ is the anisotropy parameter. For a rhombic tensor,

$$I(\omega) = \pi^{-1}[(\omega_3 - \omega_2)(\omega - \omega_1)]^{-1/2}K\left\{\arcsin\left[\frac{(\omega_3 - \omega)(\omega_2 - \omega_1)}{(\omega_3 - \omega_2)(\omega - \omega_1)}\right]^{1/2}\right\} \quad \text{for } \omega_2 < \omega < \omega_3 \qquad (22)$$

$$I(\omega) = \pi^{-1}[(\omega_3 - \omega)(\omega_2 - \omega_1)]^{-1/2}K\left\{\arcsin\left[\frac{(\omega_3 - \omega_2)(\omega - \omega_1)}{(\omega_3 - \omega)(\omega_2 - \omega_1)}\right]^{1/2}\right\} \quad \text{for } \omega_1 < \omega < \omega_2 \qquad (23)$$

$I(\omega)$ is the resonance intensity, $\omega_1 = -{}^1/_2\delta(1 + \eta)$, $\omega_2 = -{}^1/_2\delta(1 - \eta)$, $\omega_3 = \delta$, $K\{\arcsin[k]\}$ is the complete elliptic integral of the first kind, and δ and η are the anisotropy and the asymmetry parameters, respectively. Axial sum and difference tensors result only from coinciding axial quadrupolar and dipolar tensors; in other cases, the asymmetry parameter is nonzero.

Hypothetical Spectra. To illustrate the repertoire of possible spectra, we calculated a series of hypothetical spectra by using two extreme quadrupolar coupling strengths, which represent the fast motion averaged (CD_3) and the static limit of deuteron. For the static limit,

(12) Wittebort, R. J.; Olejniczak, E. T.; Griffin, R. G. *J. Chem. Phys.* **1987**, *86*, 5411−5420.

(13) Haeberlen, U. *High-Resolution NMR of Solids*; Academic Press: San Diego, CA, 1976.

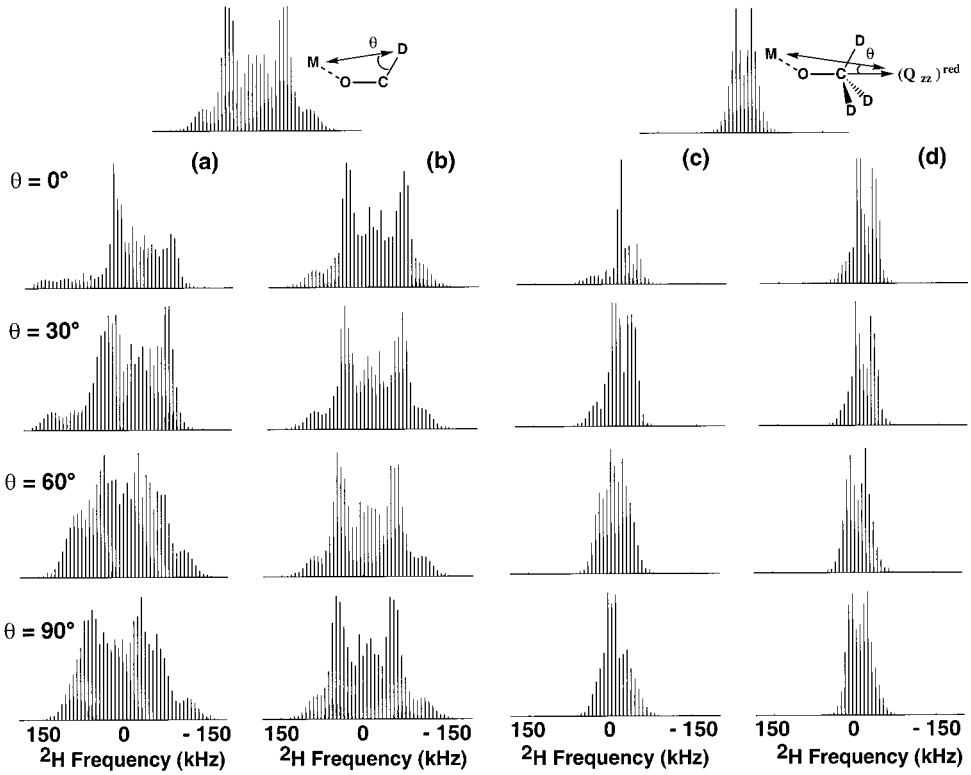

Figure 5. Simulated ^{2}H NMR lineshapes in the static and fast limit, high-symmetry motion regimes. For a static deuteron, the quadrupolar coupling constant $\omega_Q/2\pi = 167$ kHz. The spectra were simulated as a function of mutual tensor orientation, described by the polar angle θ, using (a) a dipolar coupling constant of 30 kHz and (b) a dipolar coupling constant of 5 kHz. For the fast limit, three-site hop of the methyl groups, $(\omega_Q/2\pi)_{\text{effective}} = 61$ kHz. The spectra were simulated as a function of mutual tensor orientation, described by the polar angle θ, using (c) a dipolar coupling constant of 15 kHz and (d) a dipolar coupling constant of 5 kHz. A spinning speed of 7 kHz was chosen for the simulations. The tensor orientations are defined by Euler angles between the deuterium bond and the metal−deuterium vector. Molecular motion and quadrupolar coupling strengths affect the final spectra, as is apparent from the cartoons.

the quadrupolar coupling constant was $(\omega_Q/2\pi) = 167$ kHz and $(\omega_Q/2\pi)_{\text{eff}} = 61$ kHz for the case of fast motion where $\omega_Q/2\pi = e^2qQ/\hbar$. The orientations of the dipolar and quadrupolar tensors were varied from 0° to 90°, and the dipolar coupling constants were varied from 5 to 15 kHz.

Preparation of Deuterated Compounds. V^{III}(acac-*3*-*d*)$_3$ and Cu^{II}-(DL-alanine-*d*)$_2$·D_2O were prepared as described.[14] (*N*,*N*-Ethylenebis-(salicylaldiminato))acetato-d_3-iron(III)[15,16] and *N*-isopropylsalicylaldimine-*d*-iron trichloride were prepared according to refs 15 and 16.

^{2}H NMR Experiments. All solid-state NMR spectra were recorded on a Chemagnetics CMX 400-MHz spectrometer equipped with a 5-mm CPMAS double-resonance probe. ^{2}H spectra were acquired by using either a Bloch decay or a chemical shift echo pulse sequence, with the 180° pulse synchronized with the first rotor echo at room temperature and −75 °C. The deuterium 90° pulse length was 3 μs, the dwell time was 1 μs, and recycle delay ranged from 500 ms to 2 s, depending on the compound. The instrumental sensitivity to the symmetric spectra with respect to the carrier frequency was confirmed with *d*-glycine sample and by performing electronic tests. The spinning speed was varied from 7 to 10 kHz. The data were processed in Mathematica (Wolfram Research) for a PC using a built-in FFT algorithm. The data were cut to the first rotor echo; 20-Hz exponential linebroadening was applied.

Results

Deuterium MAS SSNMR Experiments. Deuterium MAS spectra of the model compounds were measured at several spinning speeds in order to get an extensive profile of lineshapes. We believe that this collection of spectra provides strong constraints for our simulations of the electron−nuclear geometry. A 3-μs, 90° pulse produced an excitation bandwidth broad enough to cover the entire spectral width. The centerband position was determined by comparing NMR spectra corresponding to different spinning speeds. The spectra were acquired at two different temperatures (room temperature and −75 °C), since the deuterium lineshape of a paramagnetic species is expected to be affected by temperature as well.

The deuterium lineshapes of paramagnetic and diamagnetic compounds are contrasted in Figure 2. The paramagnetic compounds exhibited asymmetric lineshape in deuterium MAS NMR spectra, while symmetric lineshapes are characteristic of diamagnetic compounds. The width of deuterium sideband envelope depends on the motion of deuterons; methyl groups exhibited much narrower sideband patterns than those of deuterons in the static limit. Spectra of tris(acetylacetonato-d_3)-manganese(III) were collected at four different spinning speeds (7, 8, 9, and 10 kHz) and two temperatures (room temperature and −75 °C) (Figure 3). The sideband pattern is dependent on both temperature and spinning speed, as is illustrated by the spectra of tris(acetylacetonato-d_3)manganese(III) (Figure 3).

"Hypothetical" Simulated Static and MAS Deuterium Spectra. Calculating the MAS spectra can be time-consuming (many minutes on a 300-MHz processor) due to a discrete averaging over a large number of orientations. On the other hand, generating the static lineshapes is much faster. Static spectra can serve the purpose of sampling a large number of parameters (mutual orientations of the tensors and tensor

(14) Liu, K.; Ryan, D.; Nakanishi, K.; McDermott, A. *J. Am. Chem. Soc.* **1995**, *117*, 6897−6906.
(15) Arafa, I. M.; Goff, H. M.; David, S. S.; Muroh, B. P.; Que, L. *J. Inorg. Chem.* **1987**, *26*, 1779.
(16) Lewis, J.; Mabbs, F. E.; Richards, A.; Thornley, A. S. *J. Chem. Soc. A* **1969**, 1993.

Table 2. Parameters Characterizing the Molecular Geometry of the Model Compounds Used in This Study and Generating the Best Fit in the Simulations

compound	metal−deuterium distance, Å[a]	quadrupolar coupling constant, $\omega_Q/2\pi$ (kHz)	asymmetry parameter (η)	polar angle θ[b]	spin state
V^{III}(acac-*3*-*d*)$_3$	4.2 (5.0)	167	0	0	1
Cu^{II}(DL-alanine -*Nd*$_2$)$_2$·D_2O	2.31 (10.0)	190	0.2	35	$^1/_2$
Mn^{III}(acac-*3*-*d*)$_3$	4.3 (15 (RT[c])/40 (−75 °C))	167	0.1 (RT), 0.1 (−75 °C)	18	2
Fe^{III}(salen)(OAc-*d*$_3$)	4.87 (12.5)	56	0	15	$^5/_2$
Fe^{III}(salNiPr-*d*)Cl_3	3.43 (35.8)	175	0.1	15	$^5/_2$

[a] The value in parentheses is the dipolar coupling constant, in kHz. [b] Describing the relative orientation of the quadrupolar and the dipolar tensors. [c] RT, room temperature.

components) to restrict the parameter space, and the MAS spectra can be subsequently calculated for many fewer cases. In Figure 4, we plotted static lineshapes as a function of a dipolar coupling strength (left column), as a function of the mutual tensor orientation for a given dipolar coupling strength (middle column), and for a rhombic quadrupolar tensor. The calculated static lineshapes resemble the experimental lineshapes and were calculated using the same set of parameters as for MAS spectra.

To get an overview of the repertoire of lineshape distortions in MAS spectra for paramagnetic complexes, we also generated a series of hypothetical MAS spectra, varying the dipolar coupling strength and the tensor orientations. For this purpose, two common cases were considered: the conformationally static limit ($\omega_Q/2\pi = 167$ kHz; uniaxial) and the fast limit three-site hop ($(\omega_Q/2\pi)_{effective} = 56$ kHz; the motionally averaged tensor is also uniaxial). These two have dramatically different spectral widths. According to the simulated spectra (Figure 5), both cases showed pronounced changes in the lineshape upon varying the relative orientations of the dipolar and quadrupolar tensors from 0° to 90°. The dipolar coupling strength was also varied from 5 to 15 kHz. The distortions in the lineshape became more pronounced as the dipolar coupling strength increased, or as the effective quadrupolar coupling strength decreased through fast limit motion.

^2H Experimental and Simulated NMR Spectra of Paramagnetic Compounds. Five different selectively deuterated model compounds were chosen for lineshape fitting. The compounds allow us to demonstrate the effects of different types of motion of a deuteron and different dipolar strengths.

For the conformationally static case, tris(acetylacetonato-d_3)-vanadium(III) was selected. The simulated spectrum was compared with the experimental spectrum measured at 7 kHz spinning speed. Both spectra displayed identical spinning sideband patterns, as shown in Figure 6. The polar angle between the dipolar and the quadrupolar tensors, 0°, was obtained from the crystal structure and used for the simulation. The three deuterium atoms in the compound are in different local geometric and electronic environments due to differences in crystal packing and exhibit distinct isotropic chemical shifts but analogous spinning sideband intensity patterns. The parameters resulting in best fits are summarized in Table 2.

Another interesting and more complicated case is that of the compounds with a nonaxial electric quadrupolar tensor. Significant rhombicity in the quadrupolar tensor is often observed in compounds with strong hydrogen bonds.[17] Very asymmetric local environments involving hydrogen bonds are inherent to most of the biological solids, and therefore deuterons in such environments are likely to exhibit rhombic quadrupolar tensors. We collected and simulated ^2H MAS spectra of a model molecule, Cu^{II}(DL-alanine-*Nd*$_2$)$_2$·D_2O (Figure 7), where we expect a fairly large asymmetry parameter for the quadrupolar interaction. In this compound, the deuteron forms a strong hydrogen bond with either the adjacent O or N atoms. We

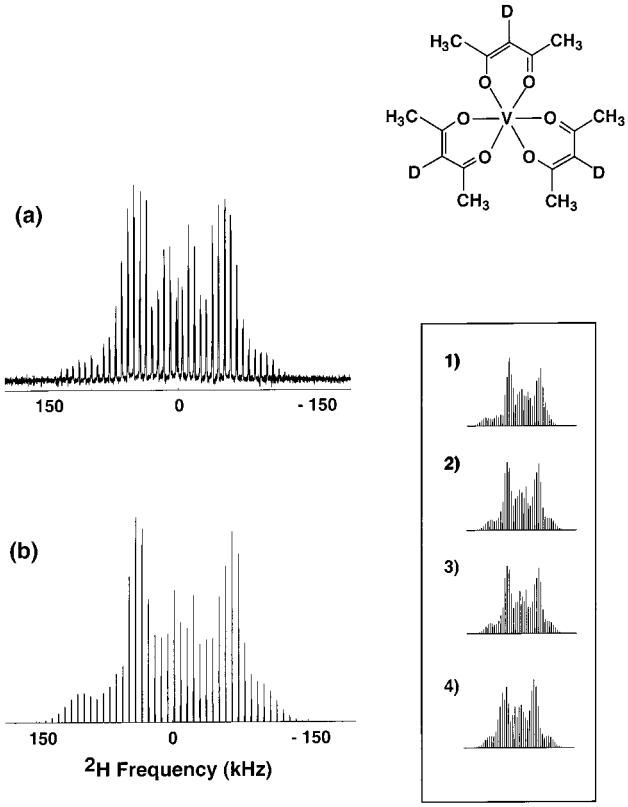

Figure 6. ^2H NMR spectra of tris(acetylacetonato-d_3)vanadium(III). (a) The experimental spectrum. The ^2H spectrum was acquired using a chemical shift echo pulse sequence, with the 180° pulse synchronized with the first rotor echo at 7 kHz spinning speed. The recycle delay was 1 s, and the sampling time was 1 μs. The three deuterium atoms in the compound have distinct isotropic chemical shifts but analogous sideband intensity pattern. (b) The simulated spectrum. The spinning sideband intensity pattern was simulated using a dipolar coupling constant of 5 kHz, based on the distance from vanadium(III) to deuterium of 4.2 Å and the quadrupolar coupling constant $\omega_Q/2\pi =$ 167 kHz, and assuming the two tensors are 0° with respect to each other, as follows from the crystal structure. The spin state of vanadium-(III) is $S = 1$ ($3d^2$), and T_1 is 5×10^{-12} s. The spinning sideband intensity pattern was simulated for one of the deuterium sites and will be analogous for the others. The rmsd from the experimental spectrum is 0.11. The inset demonstrates that the spinning sideband intensity pattern is sensitive to variation in distances by ±1.0 Å and angles by 30°. The spectra in the inset were simulated using the following parameters: (1) a dipolar coupling constant of 10 kHz, corresponding to 3.2 Å (−1.0 Å), and a polar angle θ of 0° (rmsd = 0.17), (2) a dipolar coupling constant of 3 kHz, corresponding to 5.2 Å (+1.0 Å), and a polar angle θ of 0° (rmsd = 0.11), (3) a dipolar coupling constant of 5 kHz dipolar coupling constant, and a polar angle θ of 30° (rmsd = 0.105), and (4) a dipolar coupling constant of 5 kHz, and a polar angle θ of 55° (rmsd = 0.20).

observed a pronounced effect on the NMR spectra. The spinning sideband pattern could not be reproduced assuming a uniaxial

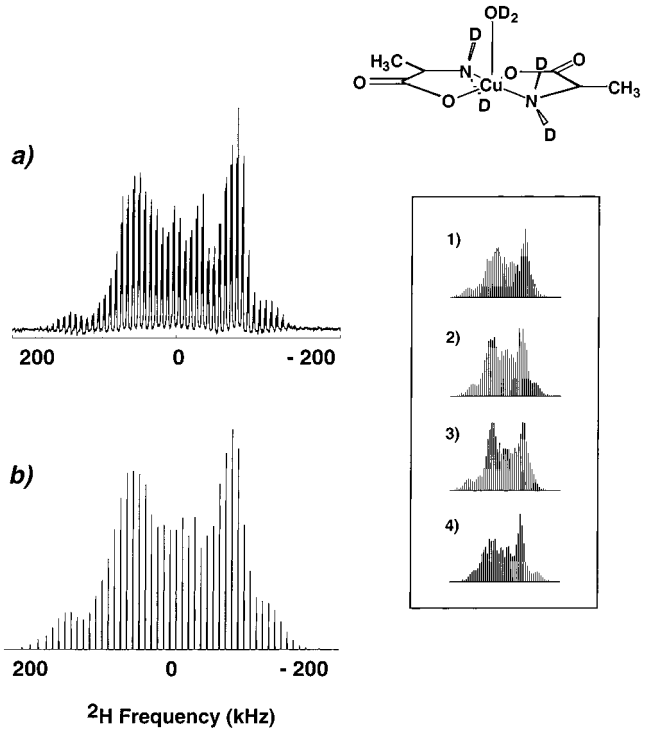

Figure 7. ^{2}H NMR spectra of *trans*-bis(DL-alaninato-N,O-*Nd*$_2$)copper-(II) monohydrate. (a) The experimental spectrum. The ^{2}H spectrum was acquired using a chemical shift echo pulse sequence, with the 180° pulse synchronized with the first rotor echo and using 7 kHz spinning speed. The recycle delay was 0.1 s, and the sampling rate was 1 μs. (b) The simulated spectrum. The spinning sideband intensity pattern was simulated using a dipolar coupling constant of 10 kHz dipolar coupling constant, a quadrupolar coupling constant $\omega_Q/2\pi$ of 190 kHz, an asymmetry parameter η of 0.2, and assuming that the two tensors are 35° with respect to each other. The spin state of copper(II) is $S = {}^1/_2$ ($3d^9$), and T_1 is $(1-3) \times 10^{-9}$ s. The spectrum was calculated by random sampling of 300 crystallites. The rmsd from the experimental spectrum is 0.07. The inset demonstrates that the spinning sideband intensity pattern is sensitive to variation in distances by ±0.5 Å and angles by 20°. The spectra in the inset were simulated using the following parameters: (1) a dipolar coupling constant of 20.9 kHz, corresponding to 1.81 Å (−0.5 Å), and a polar angle θ of 35° (rmsd = 0.10), (2) a dipolar coupling constant of 5.6 kHz, corresponding to 2.81 Å (+ 0.5 Å), and a polar angle θ of 35° (rmsd = 0.10), (3) a dipolar coupling constant of 10 kHz, and a polar angle θ of 15° (rmsd = 0.11), and (4) a dipolar coupling constant of 10 kHz, and a polar angle θ of 60° (rmsd = 0.13).

quadrupolar tensor, and a satisfactory fit could be obtained assuming the asymmetry parameter $\eta = 0.2$ (Table 2). There are two deuterium sites in the molecule, each containing a pair of deuterium atoms related by symmetry; these two sites exhibit distinct isotropic chemical shifts but analogous spinning sideband intensity patterns.

We observed significant changes in the lineshape upon changing the temperature and spinning speed for Mn(acac-*d*)$_3$ (Figure 3). To evaluate the accuracy of the simulations, we attempted to fit the spinning sideband intensities of the MAS spectrum of Mn(acac-*d*)$_3$. Spectra collected at different temperatures and spinning speeds were simulated (Figure 8). First, we found that the best fits of the spectra at the spinning speeds from 7 to 10 kHz at room temperature required the use of a dipolar coupling constant of 15 kHz and a quadrupolar coupling constant $(\omega_Q/2\pi)_{\text{effective}} = 167$ kHz, with the asymmetry parameter $\eta = 0.1$. The slight discrepancies between the experimental and the simulated spectra may be due to sample inhomogeniety coming from the fact that two different types of crystal packing exist for Mn(acac-*d*)$_3$.[18]

For spectra collected at −75 °C, we were obliged to use a stronger dipolar coupling constant of 40 kHz to successfully simulate the experimental spectra. This result is not surprising: the Curie factor is a function of temperature, and the effective moment of the electron is stronger at low temperatures. Therefore, good agreement between the experiment and simulation can be obtained for this more complex case using our simplified model.

N-Isopropylsalicylaldiminate-*d*-iron(III) trichloride (a, shown below) was synthesized and characterized by X-ray crystal logography.[19] We could not fit the experimental spinning sideband

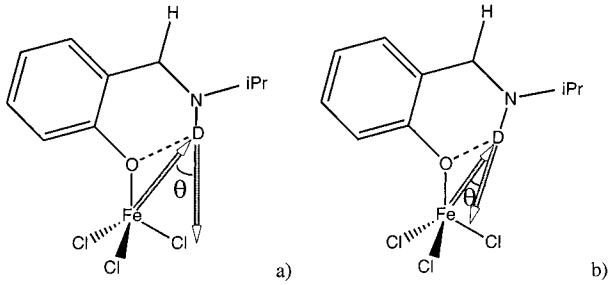

intensities using the tensor information based on distances obtained from the crystal structure. Therefore, we attempted to use slightly different relative tensor orientations and dipolar coupling strengths. The parameters used in the simulations are specified in the caption of Figure 9. The resulting fit (Figure 9; the fit parameters are summarized in Table 2) is close to the experimental spectrum. Based on the simulation, we found that the distance from iron(III) to deuterium was 3.64 Å, assuming that the spin state of iron(III) is $S = 5/2$. Due to the geometry of the deuteron (shared between the N and the O), significant rhombicity in the quadrupolar interaction tensor is expected. The simulations agree with this prediction, and the best fit is generated using $\eta = 0.1$. The polar angle was calculated to be 15° on the basis of the simulation, rather than 30° as measured from the crystal structure. However, these discrepancies can be explained chemically in the following manner: The distance between the deuteron and the neighboring oxygen shortens due to the formation of a hydrogen bond between the two (shown in b). This leads to a longer distance between Fe(III) and the deuteron and a smaller angle between the N−D bond and the Fe(III) vector. In this case, a nonzero asymmetry parameter for the quadrupolar tensor is also expected, in agreement with the simulations. The discrepancies between the simulation parameters and the crystal structure are not very surprising: that the hydrogen positions in the crystal structures are inaccurate is a well-known fact, and this inaccuracy introduces additional errors in the estimates of angles and coupling strengths. Thus, this simulation method is capable of refining proton (deuteron) positions.

Figure 10 shows the experimental and simulated spectra of motionally averaged deuterium in a methyl group. (*N*,*N*′-Ethylenebis(salicylaldiminato))acetato-d_3-iron(III) was chosen as a model compound. The deuterons of the methyl group in this molecule exhibit fast limit three-site hop motions. The best fit to the experimental spectrum was generated using the parameters which correspond to the molecular geometry shown in Figure 10 (the fit parameters are summarized in Table 2). The principal axes of the quadrupolar and the dipolar tensors are 15° with respect to each other, and the coupling strengths are as follow: the quadrupolar coupling constant $(\omega_Q/2\pi)_{\text{effective}}$

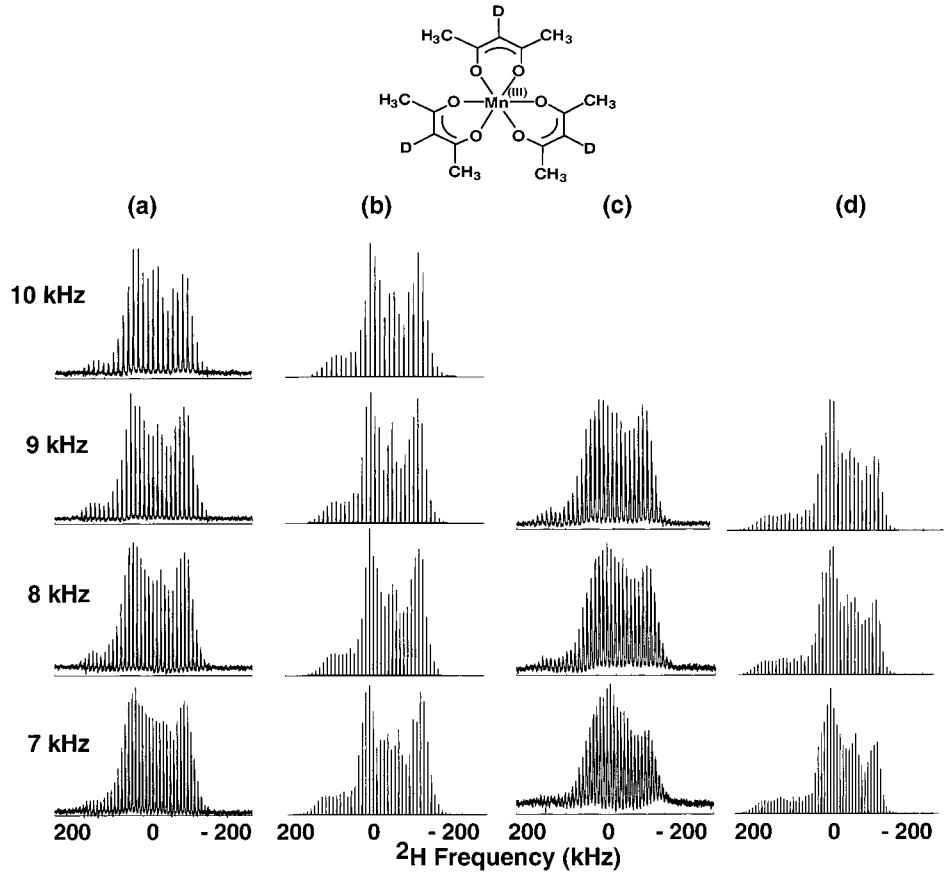

Figure 8. ^2H NMR spectra of tris(acetylacetonato-d_3)manganese(III). (a) An experimental spectrum. The ^2H spectrum was acquired using a chemical shift echo pulse sequence, with the 180° pulse synchronized with the first rotor echo. The sample was spun at 7−10 kHz at room temperature. (b) A simulated spectrum. The spinning sideband intensity pattern was simulated using a dipolar coupling constant of 15 kHz (based on the distance from manganese(III) to deuterium of 4.3 Å), a quadrupolar coupling constant $\omega_Q/2\pi$ of 167 kHz, an asymmetry parameter η of 0.1, and a polar angle θ of 18°. The spin state of manganese(III) is $S = 2$ ($3d^4$), and T_1 is 10^{-11}−10^{-10} s. The rmsd from the experimental spectra are 0.12, 0.11, 0.11, and 0.10 for the spinning speeds of 7, 8, 9, and 10 kHz, respectively. (c) An experimental spectrum. The sample was spun at 7−10 kHz at −75 °C. (d) A simulated spectrum. The spectrum was simulated using a dipolar coupling constant of 40 kHz. The rmsd from the experimental spectra are 0.11, 0.13, and 0.18 for the spinning speeds of 7, 8, and 9 kHz, respectively.

= 56 kHz, and the dipolar coupling constant is 12.5 kHz, implying a distance of 4.87 Å between the iron center and the conformationally averaged deuterons. A recently reported crystal structure of the compound[20] reveals that it forms linear polymer chains, as shown in the cartoon below:

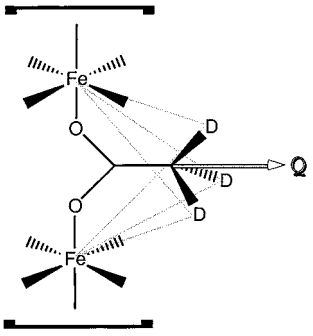

It appears from the geometry that, for each methyl group in the molecule, two equidistant irons will contribute to the electron−nuclear dipole coupling. This gives rise to partial averaging of the effective dipolar vector, resulting in a weaker apparent dipolar coupling constant, a longer apparent distance from the iron center to the deuterons, and a small apparent angle between the quadrupolar and the dipolar tensors, in agreement with the simulations.

Discussion

Validity of the Approximations Used in the Simulations. The following approximations were adopted for the simulations:

(1) The anisotropic part of the interaction between the electron and the deuteron is of a purely dipolar origin; the chemical shift anisotropy was assumed to be negligible.

(2) The electronic magnetic moment is localized on the metal, and a point dipole approximation can be used to describe the electron−nuclear dipolar interaction.

(3) The electron spin relaxation is much faster than the nuclear spin transitions, and therefore the electron spin states can be described by the averaged magnetic moment.

(4) The isotropic part only of the $\tilde{\mathbf{g}}$-anisotropy tensor was preserved.

The electron−nuclear dipole−dipole coupling is the largest anisotropic interaction that contributes to the asymmetric lineshapes and spinning sideband intensities in the spectra. The Fermi contact term (electron−nuclear exchange interaction) might also be significant and is often responsible for large paramagnetic chemical shifts. This is probably an isotropic interaction, and therefore it was assumed to not affect the

(17) Hunt, M. J.; Mackay, A. L. *J. Magn. Reson.* **1974**, *15*, 402−414.
(18) Fackler, J. P., Jr.; Avdeef, A. *Inorg. Chem.* **1974**, *13*, 1864−1875.
(19) Beer, R. H.; Kisko, J. Manuscript in preparation.
(20) Liu, G.; Arif, A. M.; Bruenger, F. W.; Miller, S. C. *Inorg. Chim. Acta* **1999**, *287*, 109−112.

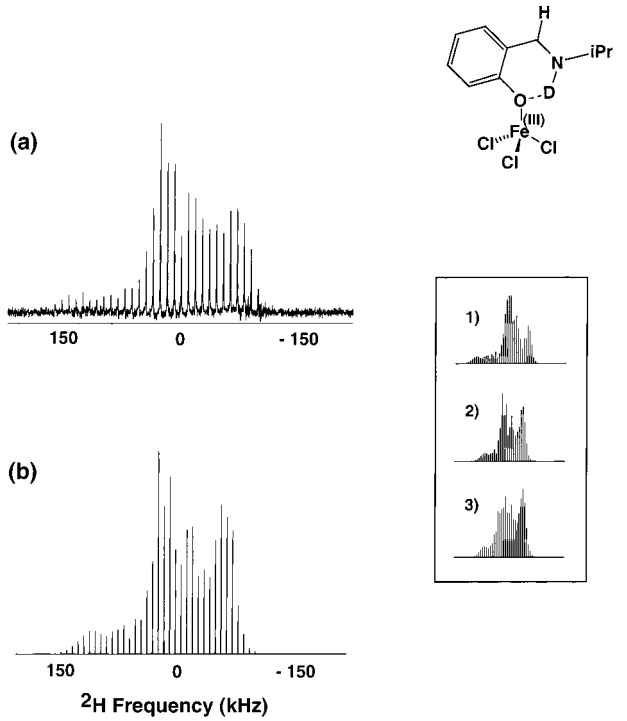

Figure 9. ^{2}H NMR spectra of *N*-isopropylsalicylaldiminato-*d*-iron-(III) trichloride. (a) An experimental spectrum. The ^{2}H spectrum was acquired using a Bloch decay; the sample was spun at 10 kHz. The recycle delay was 0.1 s, and the sampling rate was 1 μs. (b) A simulated spectrum. The spectrum was simulated using a dipolar coupling constant of 35.8 kHz, a quadrupolar coupling constant $\omega_Q/2\pi$ of 190 kHz, a polar angle θ of 15°, and an asymmetry parameter η of 0.1. The spin state of iron(III) was assumed to be $S = {}^5/_2$ ($3d^5$). The rmsd from the experimental spectrum is 0.08. The inset demonstrates that the spinning sideband intensity pattern is sensitive to variation in distances by ±0.5 Å and angles by 20°. The spectra in the inset were simulated using the following parameters (for all the spectra in the inset, $\omega_Q/2\pi$ of 175 kHz, and η of 0.1 were used): (1) a dipolar coupling constant of 47 kHz, corresponding to 3.14 Å (−0.5 Å), and a polar angle θ of 15° (rmsd = 0.13), (b) a dipolar coupling constant of 20 kHz corresponding to 4.14 Å (+0.5 Å), and a polar angle θ of 15° (rmsd = 0.16), and (c) a dipolar coupling constant of 30 kHz, and a polar angle θ of 35° (rmsd = 0.19).

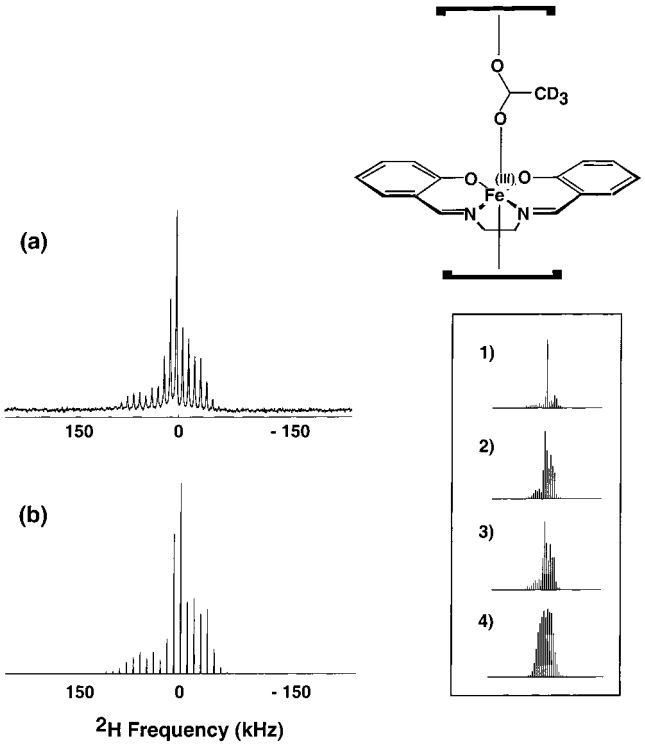

Figure 10. ^{2}H NMR spectra of (*N*,*N*′-ethylenebis(salicylaldimine))-acetato-d_3-iron(III). (a) An experimental spectrum. The ^{2}H spectrum was acquired using a chemical shift echo pulse sequence, with the 180° pulse synchronized with the first rotor echo and using 7 kHz spinning speed. The recycle delay was 0.1 s, and the sampling rate was 1 μs. (b) A simulated spectrum. The spectrum was simulated using a dipolar coupling constant of 12.5 kHz, a quadrupolar coupling constant $\omega_Q/2\pi$ of 56 kHz, and a polar angle of 0°. The spin state of iron(III) is $S = {}^5/_2$ ($3d^5$), and T_1 is 10^{-11}−10^{-10} s. The rmsd from the experimental spectrum was 0.05. The inset demonstrates that the spinning sideband intensity pattern is sensitive to variation in distances by ±0.5 Å and angles by 20°. The spectra in the inset were simulated using the following parameters: (1) a dipolar coupling constant of 17.3 kHz, corresponding to 4.37 Å (−0.5 Å), and a polar angle θ of 0° (rmsd = 0.15), (2) a dipolar coupling constant of 9.3 kHz, corresponding to 5.37 Å (+0.5 Å), and a polar angle θ of 0° (rmsd = 0.15), (3) a dipolar coupling constant of 12.5 kHz, and a polar angle θ of 20° (rmsd = 0.16), and (4) a dipolar coupling constant of 12.5 kHz, and a polar angle θ of 55° (rmsd = 0.37).

anisotropy of the lineshapes. The other anisotropic terms (such as chemical shift anisotropy, CSA) are negligibly small and can be safely disregarded.

The second assumption, the point dipole approximation, appears to be valid in systems where the nucleus is at a relatively long distance from the paramagnetic center. In practice, this implies more than two-bond separation between the electron and the nucleus. Otherwise, the symmetry of the metal orbitals most likely has to be taken into consideration when constructing the dipolar Hamiltonian. In most of the paramagnetic compounds whose NMR spectra we acquired and simulated, the metal center was at least four bonds away from the deuterium nucleus; therefore, the point dipole approximation was reasonable. In Cu^{II}(DL-alanine-*d*)$_2$·D_2O, deuterium is separated from the metal center by only two bonds, and the point dipole approximation may no longer be valid. Nonethless, in these simulations we kept this approximation to avoid introducing extra free parameters. As is apparent from Figure 7, good fits to the experimental spectra were obtained, despite the use of this simplifying assumption.

Treating the electronic spin states as the thermally averaged mean magnetic moment is a common description[10,11] and is valid for our experimental conditions, where the high-temperature limit is reached.

The most severe approximation used in the simulations was to disregard the $\tilde{g}$-anisotropy, whose presence introduces additional line broadening in the spectra and may affect the lineshape. If the *g*-anisotropy is small or moderate (<5%), then its effect on the deuterium NMR spectra can be neglected to a good approximation. Otherwise, the *g*-anisotropy would have to be taken into account. A rigorous treatment requires extending the dimensionality of the tensorial interactions up to the sixth rank in the following manner. The $\tilde{g}$-anisotropy and the dipolar interactions are second-rank tensors, and the combined interaction tensor, which will be used for constructing the dipolar Hamiltonian (eq 6), will contain the direct (outer) product of these tensors, in the form

$$\tilde{T}_{\mathrm{dip}} = \left(\frac{\beta^2 S(S+1)}{3k_{\mathrm{B}}T}H_0\right)(\tilde{g}\otimes\tilde{g}\otimes\tilde{D}) \qquad (24)$$

or, in the spherical tensor notation,

$$(\tilde{T}^J_M)_{\mathrm{dip}} = \frac{\beta^2 S(S+1)}{3k_B T} H_0 \sum_{m_1}\sum_{m_2}\sum_{m_3} C^{JM}_{(j_1+j_2)(m_1+m_2);j_3 m_3} C^{(j_1+j_2)(m_1+m_2)}_{j_1 m_1; j_2 m_2} (\tilde{g}^{j_1}_{m_1})^{\mathrm{CFF}} (\tilde{g}^{j_2}_{m_2})^{\mathrm{CFF}} (\tilde{D}^{j_3}_{m_3})^{\mathrm{CFF}} \quad (25)$$

where $C^{JM}_{j_1 m_1; j_2 m_2}$ are the Clebsch−Gordon coefficients for coupling of two spherical tensors,[21] and T^j_m is a $\{j,m\}$ component of the corresponding tensor (i.e., *g*-anisotropy, dipolar tensor, or the combined interaction tensor, which must all be expressed in a common molecular frame (CFF)). Typically, we know these interactions in their principal axes system (PAS), and they are placed in the CFF by a rotation. In the spherical tensor notation, j is the total angular momentum and m is its projection onto the *z*-axis: $m = -j, -j+1, ..., 0, ..., j-1, j$. The individual interactions are represented by the second rank tensors. Therefore, tensors of up to sixth rank will be generated according to eqs 23 and 24 and will contribute to the final expressions for the MAS spectra.

Equation 25 describes interactions in a CFF. These tensor components must then be rotated to the laboratory frame (LAB), typically in two steps: by first placing crystallites in the rotor (and generating a powder pattern at this step), and by then performing a second time-dependent rotation from the rotor fixed frame (RFF) to LAB. In the LAB frame, truncation to the *z*-component only is performed. The expression for the resonance frequency in the LAB frame will thus be obtained and used to generate the MAS spectra analogously to ref 7. As is true for quadrupolar nuclei, time-independent but spatially anisotropic terms will result from these tensors during MAS. Incomplete refocusing of the anisotropic components of frequency in the presence of $\tilde{g}$-anisotropy results in additional inhomogeneous linebroadening of each of the spinning sidebands: unlike the second-rank case, the higher-rank frequency components cannot be averaged out by spinning at the "magic angle" of 54.7°. Work to incorporate the $\tilde{g}$-anisotropy tensor into the simulations is in progress. Nonetheless, at the beginning of this study, to a very crude approximation, we disregarded the $\tilde{g}$-anisotropy and included only the isotropic part of the interaction into our calculations. As is evident from Figures 6−10, a good agreement between the experimental and the simulated spectra is reached, even for the compounds known to exhibit significant *g*-anisotropy [Fe^{III}(salNiPr-*d*)Cl_3 and Fe^{III}-(salen)(OAc-d_3), Figures 9 and 10], probably because of extensive electron−electron spin exchange in these neat solids. Currently, we are including the $\tilde{g}$-anisotropy in the simulations (to be reported elsewhere).

Information Content of the Simulated Spectra and Quality of the Fits. The lineshapes reflect the local molecular geometry, as they are dominated by strong anisotropic dipolar interactions between the deuteron and the thermally averaged magnetic moments of the unpaired electrons, and they also reflect motion. The strength of the dipolar interaction affects the extent of asymmetry in the lineshapes of the deuterium NMR spectra. Depending on the distance between the metal center and the deuteron, and on the spin state of the metal, the dipolar coupling strength may range from several kilohertz to 100 kHz, and in certain cases it may approach or even exceed the strength of the deuterium quadrupolar coupling (167 kHz for the static deuterium and 56 kHz for motionally averaged deuterium undergoing a three-site hop in CH_3 groups). Dipolar couplings as weak as 5 kHz can be detected by these simulations. This corresponds to the distance between the metal and the deuteron(s) of 3 Å for $S = {}^1/_2$ and 6.5 Å for $S = {}^5/_2$ systems. In other words, the deuterons 3−5 bonds away from the metal center can be detected for $S = {}^1/_2$ to $S = {}^5/_2$ systems, respectively. Specific preferences for a given rotamer in systems exhibiting symmetry-related motions can also be pronounced in the deuterium MAS spectra of paramagnetic compounds, and the simulations can unambiguously distinguish the preferred rotamer.

The spectral lineshape reflects the mutual orientation of the dipolar and the quadrupolar tensors, and the breadth of the spectral envelope indicates the effective strength of the quadrupolar coupling. Each of the local geometry parameters is related to a specific feature of the deuterium NMR spectrum, and therefore, one anticipates that a single NMR spectrum would provide simultaneous estimates on all the parameters. Curiously, a preliminary idea of the possible range of values can be obtained by simply looking at the MAS spectrum. This is illustrated in Figures 4 and 5, where we showed the influence of the dipolar coupling strength and the polar angle on the spectral lineshape for each of the two transitions, assuming axial quadrupolar and dipolar interactions. Interestingly, the rhombic quadrupolar interaction also gives rise to unique features in the paramagnetic MAS spectra, as shown in Figures 4 and 5.

To test how changes in each of the parameters would affect the spectra in practice, we consider the model compounds. We performed a series of simulations in which we independently varied the dipolar coupling strength and the polar angle. As was discussed above, for each of the model compounds those two parameters were known from the crystal structure. The results of the simulations are shown in Figures 6, 7, 9, and 10. As is apparent from the figures, the MAS spectra are very sensitive to both the dipolar coupling strength and the angle. The measurements allow to discriminate distances of ±0.5 Å and angles of ±20° for the strong coupling regimes (>5 kHz) but are more tolerant to the distance and the angle variations for the weaker coupling regimes, such as V^{III}(acac-*3*-*d*)$_3$ (5 kHz), as expected.

The above simulations also served the purpose of addressing the quality of the fits. This will become especially important in systems whose fine structure constants are not known a priori and are to be assessed from the deuterium spectra and subsequent simulations. For such systems, large parameter space will have to be sampled in order to obtain the best fit. Our initial approach (reported in this manuscript) was aimed at understanding whether it will be possible to generate a unique fit on the basis of a range of probable values for the fine structure constants, and what the expected accuracy of the method is. It appears that a unique answer can be obtained, and an automated search will be beneficial. Despite the fact that the lineshapes offer unique fits and natural separation of fitting variables, we are nonetheless interested in developing automated fitting procedures that will offer statistical figures of merit. Monte Carlo-based algorithms will be employed for searching the multiparameter space; this work is in progress.

Future Applications. Deuterium MAS spectra of paramagnetic compounds contain valuable information about the local dynamics and fine structure constants, as illustrated above. The method appears to have enough sensitivity for applications in large paramagnetic biological systems, where such measurements would often be the only means of addressing the local geometry of the paramagnetic environment. We have already performed experiments on two paramagnetic metalloprotein−ligand complexes[2,3] and have obtained information about the

(21) Rose, M. E. *Elementary Theory of Angular Momentum*; Dover Publications: Mineola, 1995.

substrate geometry and dynamics in the active site of these enzymes. An interesting and important feature of deuterium MAS spectra of paramagnetic solids is their sensitivity to the hydrogen position within a given molecule, which can be indispensable for accurate positioning of hydrogen bonds, for identification of the geometry of substrate motions within enzymes, and for other applications. The method offers the advantage of moderate and variable temperature conditions, as compared with EPR techniques traditionally used to extract this kind of information.[22−27]

For biological systems, low sensitivity is very often a serious issue. One of the possibilities to alleviate the problem is to apply noise reduction protocols. The noise filtering technique for deuterium MAS spectra developed in our laboratory and described by Liu et al.[2] demonstrates a severalfold enhancement in the signal-to-noise ratio. Another possibility is 1D-to-2D filtering, which in addition to increasing the signal-to-noise ratio offers the advantage of separating the peaks in the deuterium spectrum according to their isotropic chemical shifts, which can be important for the MAS spectra with multiple resonances.[28]

(22) Burdi, D.; Willems, J. P.; Riggs-Gelasco, P.; Antholine, W. E.; Stubbe, J.; Hoffman, B. M. *J. Am. Chem. Soc.* **1998**, *120*, 12910−12919.
(23) Davydov, R.; Valentine, A. M.; S., K.-P.; Hoffman, B. M.; Lippard, S. J. *Biochemistry* **1999**, *38*, 4188−4197.
(24) Diner, B. A.; Force, D. A.; Randall, D. W.; Britt, R. D. *Biochemistry* **1998**, *37*, 17931−17943.
(25) Elliott, S. J.; Randall, D. W.; Britt, R. D.; Chan, S. I. *J. Am. Chem. Soc.* **1998**, *120*, 3247−3248.
(26) Peloquin, J. M.; Tang, X. S.; Diner, B. A.; Britt, R. D. *Biochemistry* **1999**, *38*, 2057−2067.
(27) Willems, J. P.; Valentine, A. M.; Gubriel, R.; Lippard, S. J.; Hoffman, B. M. *J. Am. Chem. Soc*. **1998**, *120*, 9410−9416.
(28) Brown, S. P.; Heyes, S. J.; Wimperis, S. *J. Magn. Reson.* **1995**, *119*, 280−284.

Conclusions

Deuterium MAS spectra of paramagnetic systems bear information about the local geometry and dynamics. Simulations of the NMR spectra allow us to extract all of the fine structure constants simultaneously, as each of the parameters gives rise to a unique feature in the lineshape. We simulated the experimental spectra for model compounds and showed that good agreement between the experiment and the calculations can be reached using the fine structure constants obtained from the crystal structure. We assessed the sensitivity of MAS spectra to the fit parameters and demonstrated that distances of ± 0.5 Å and angles of $\pm 20°$ can be easily distinguished between. This method has the potential for characterizing the metal centers in paramagnetic biological systems, under conditions complementary to those used in EPR studies.

Acknowledgment. The authors thank Dr. Kai Liu (UC Berkeley) for her feedback and discussions of the project, and Tony Hascall and Professor Gerard Parkin (Columbia University) for their help with metrical data from the X-ray crystal structure of Fe^{III}(salNiPr-*d*)Cl_3. Financial support of this work was provided by NIH (Grant GM-49964), DOE (Grant DE-FG02-95ER14508), the Kanagawa Academy of Science and Technology, and a grant to the Columbia Environmental Molecular Sciences Institute from the National Science Foundation and the Department of Energy, Grant NSF CHE 98-10367 (A.E.M.). A.E.M. is a Cottrell Scholar of Research Corp. This manuscript is dedicated to the memory of Professor Regitze Vold in honor of her scientific leadership in deuterium NMR spectroscopy and NMR studies of biological systems.

JA990636U